Q-ENHANCEMENT OF PIEZO-ON-SILICON MEMS RESONATORS THROUGH MODE-COUPLING AND TOPOLOGICAL TANK CONFIGURATIONS

Suaid Tariq Balghari, Abid Ali, and Frederic Nabki
Department of Electrical Engineering, École de Technologie Supérieure, Montréal, Canada

ABSTRACT

This study presents a technique for enhancing the quality factors *(Q)* in traditionally low *Q* exhibiting thin-film piezoelectric on substrate (TPoS) resonators through mechanical coupling with single crystalline silicon (SCS) structures in a tank topology. Using this methodology, quality factors of 46,503 and 19,338 have been obtained for the novel Button-like mode coupled to four shear mode disks exhibiting a 10X improvement in unloaded quality factor Q_{ul} compared to a standalone button-like mode. Design considerations are proposed to achieve high *Q* values through mechanical coupling in tank configuration through optimum mode selection and the appropriate coupling location.

KEYWORDS

Micro-electro-mechanical systems (MEMS), Resonators, Piezoelectric, Quality factor, Motional resistance, Timing, Coupled mode

INTRODUCTION

Micro-electro-mechanical (MEM) resonators have often been considered the leading candidates to replace legacy Quartz crystal resonators to meet the miniaturizing footprint demands of integrated electronics for various applications[1]. However, MEMS resonators must exhibit the stringent performance levels achieved by high-performance crystal resonators. The two main categories of MEMS resonators have their merits as well as shortcomings. Capacitive resonators have already matched quality factors *(Q)* of piezoelectric quartz crystals yet the high motional resistance (R_m) along with issues of non-linearity pose obstacles. On the flip side, piezoelectric MEMS resonators exhibit low R_m but cannot compare in *Q* values. Thin-film piezoelectric on substrate (TPoS) devices have emerged as a viable option to counter the shortcomings of the two transduction mechanisms [2]. However, while a lower R_m has been obtained via a stronger coupling coefficient (k_t^2), the presence of an additional layer has resulted in a lower *Q* in comparison to a single-crystal silicon (SCS) resonator [3]. A high *Q* is essential to reduce the close-to-carrier frequency phase noise in oscillators [4]. Hence, for timing and frequency reference applications, a high-quality factor becomes indispensable.

Research efforts to enhance the low *Q* of TPoS resonators brought forth mechanically coupled arrays of TPoS resonators with electrode-less structures to boost the energy storage of the overall resonator [3]. Recently, mechanical coupling of traditionally high *Q* exhibiting Lame modes with a piezoelectrically transduced length extensional (LE) mode achieved significant improvements in quality factors [5]. Similarly, the extension of this concept in 2-D arrays of Lame modes achieved remarkable frequency-quality factor product *f.Q* values for TPoS resonators [6].

This work, while building upon these efforts, attempts to present design considerations for optimized mechanical coupling. The device constitutes a piezoelectrically driven silicon resonator mechanically attached to SCS structures in a tank topology. In contrast to the above-mentioned works, our devices employ non-conventional modes that are optimized for a tank configuration targeting *Q*-boosting. Finite element simulations have been performed to further explore the technique where two different mode configurations have been compared. Low-cost commercial fabrication technology has been employed to validate the concepts. The experimental results have been presented to validate the methodology. The influence of environmental perturbation has been shown on the *Q* of the resonator and a comparison with the state-of-the-art has been presented in the conclusion.

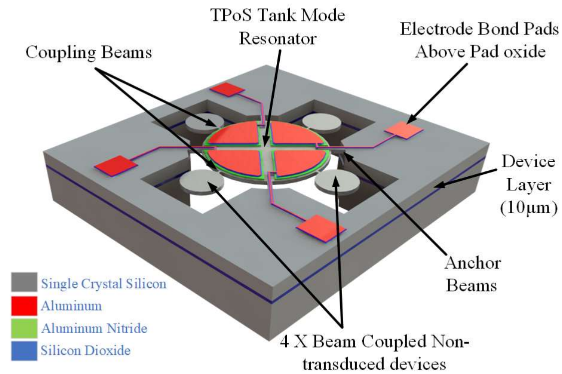

Figure 1: 3D representation of the stack of structural layers of the proposed TPoS resonator operating in a 4-port differential transduction scheme.

DESIGN OF TANK MODE RESONATOR

A 3-dimensional rendering of the proposed design is shown in Fig. 1 wherein a central TPoS disk has been coupled to 4 small SCS disks through narrow mechanical beams. The central TPoS tank comprises a 10-micron silicon device layer, on top of which a thin 0.5 μm aluminum nitride layer has been deposited which is further layered with aluminum acting as the top electrode. The piezoelectric thin film and the metal electrodes are arranged in a fan-like 4-port layout for a fully differential transduction mechanism. Thus, the central tank has a differential strain profile which aids in nullifying the feed-through capacitance resulting in a stronger output signal. This tank has been mechanically coupled to 4 single crystal silicon structures along the <100> crystallographic axes.

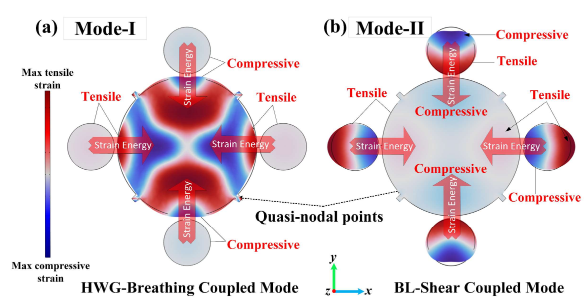

Figure 2: Differential modes under comparison (a) Strain profile for higher wineglass (HWG) tank mode coupled to 4 breathing modes with red arrows indicating the acoustic strain energy reflection towards central tank (b) Strain profile for button-like mode coupled to 4 shear modes.

To test the validity of *Q*-enhancement methodology as well as to outline critical design aspects, two different mode pairs are analyzed as shown in Fig. 2. Eigenfrequency simulations have been

978-1-940470-05-4/HH2024/$25©2024TRF
DOI 10.31438/TRF.HH2024.10

performed in COMSOL Multiphysics to obtain the mode shapes which are essential to determine the electrode placements for optimum mode extraction. Mode-I has the HWG as the tank mode and is attached to four breathing modes as can be seen in Fig. 2 (a). Mode-II is shown in Fig. 2 (b) where the novel button-like (BL) mode [7] is the central tank appended to four disks vibrating in the shear mode. Areas of tensile and compressive strains on the respective modes have been indicated along with the nodal points for anchoring. The specific mode shapes have been obtained by appropriate selection of the disk diameters obtained through frequency matching. Fig. 2 also visually depicts the quality factor enhancement methodology, in which the 4 SCS disks act as acoustic reflecting structures to minimize strain energy dissipation from the central tank. Such a concept has been previously demonstrated for anchor loss mitigation [8], where cavities in the substrates forced an impedance mismatching to minimize strain transference from the anchoring tethers. In our case, instead of acoustic cavities, vibrating structures are being utilized for the same purpose.

The performance improvement technique also dictates the mode appropriation for the device. While the central tank resonance mode has been chosen to be differential to improve the electromechanical signal strength which brings down overall motional impedance of the resonator, the mode shapes of the appended SCS disks have another criterion. Contrary to conventional resonator research where low anchor loss modes are preferred, the four appended disks must now exhibit higher tether loss so that this energy is transferred to the central tank via the coupling beams. To quantitatively define this design objective, a ratio Γ between the strain energy in the coupling beam U_{cplr} to the strain energy of the resonator disk U_{res} is defined:

$$\Gamma = \frac{U_{cplr}}{U_{res}} \qquad (1)$$

Using COMSOL Multiphysics, the strain energies U_{cplr} and U_{res} are obtained through the volume integration function. The calculated energy ratios for the breathing and the shear modes are tabulated in Table 1. This predicts that the shear mode reflects higher acoustic energy resulting in a higher Q enhancement potential for Mode-II.

Table 1. Simulated Γ values for the breathing and shear modes as a measure of strain energy reflection.

Operating Mode	$\Gamma = \frac{U_{cplr}}{U_{res}} \times \Delta^{*}$
Breathing mode	73.47
Shear mode	240.08

$^{*}\Delta = 1 \times 10^{-4}$

FABRICATION:

A low-cost commercial technology, PiezoMUMPs from Science [9], was employed to fabricate the devices in this work. It is a 5-mask fabrication process starting with a silicon-on-insulator (SOI) wafer of 150 mm as shown in Fig. 3 (a). The top layer is n-doped through phospho-silicate glass (PSG) for enhancing electrical conductivity. Thermally grown oxide is deposited and patterned as shown in Fig. 3 (b) to prevent electrical contacts in areas without aluminum nitride (AlN). The AlN is then RF sputtered followed by deposition, patterning and etching in Fig. 3 (c). A metal stack of 20 nm chrome and 1 µm aluminum acts as the top conducting layer. The resulting electrodes are layered through a lift-off process to form electrical pathways and bond pads in Fig. 3 (d). Lithographical etching of silicon in the next step using deep-reactive ion etching (DRIE) forms the structural components of the TPoS and SCS structures in Fig. 3 (e). Thereafter, the front side of the substrate is covered with a protective coating for the bottom side DRIE release of the structure in Fig. 3 (f). Protective coatings are dry plasma etched forming the final released structure.

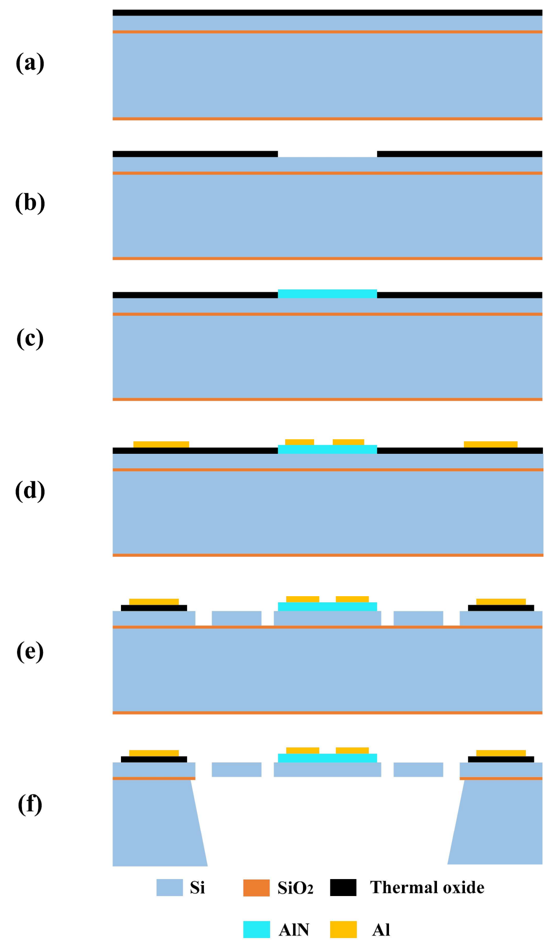

Figure 3: Process flow for fabrication process of the tank mode resonator using PiezoMUMPs: (a) Si wafer with a 10 µm handle layer. (b) Patterning of thermally grown oxide using RIE. (c) Deposition and patterning of 0.5 µm AlN using RF sputtering and RIE. (d) Deposition and patterning of a metal stack (20 nm Cr and 1 µm Al) for electrode pads and pathways. (e) Formation of device structures via DRIE down to the buried oxide layer. (f) Release of the resonating structures through bottom side DRIE with a front-side protective layer, removed by plasma etching.

The micrograph of the proposed design fabricated through this process is shown in Fig. 4. The differential transduction scheme is also depicted to obtain the desired mode while suppressing unwanted motion. Critical dimensions include the diameters of the central TPoS tank and the non-transducing SCS disks. The inset shows the width of the anchors as 16 µm which is the lowest thickness limit for metal-piezo on silicon stack in the PiezoMUMPs process. To determine the efficacy of the Q enhancement, a standalone disk was also fabricated without the non-transducing SCS structures.

MEASUREMENT:

A vector network analyzer (VNA) from Agilent (Keysight-E5061B) was utilized to obtain frequency domain characterization of the fabricated devices. Devices were actuated in both ambient air and partial vacuum conditions at 90 mTorr. As this VNA model is a 2-port device, signal splitters from Mini-Circuits were used for differential transduction. To extract the electrical lumped parameters, a modified equivalent circuit modeling technique was used to curve fit the measured signal with equations presented in [10].

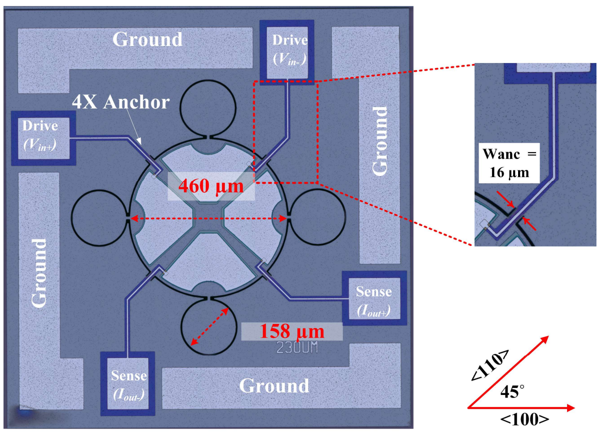

Figure 4: Micrograph of the fabricated resonator with critical dimensions and differential polarities labeled.

The measured S_{21} magnitude for the standalone HWG and BL modes is depicted in Fig. 5 (a) and (b), respectively, along with their displacement profiles. The measurements obtained for the tank mode counterparts are presented in Fig. 6 (a) and (b), respectively, along with their displacement profiles. The measured and curve-fitted plots are shown for each device, and the values of interest obtained through the curve fittings are presented in the top right of each plot. The unloaded quality factor Q_{ul} is the mechanical quality factor obtained by removing the influence of electrical loading on the device and is calculated from the loaded quality factor, Q_l, the motional resistance, R_m, and the parasitic electrical resistance, R_p, using the following equation [11]:

$$Q_{ul} = Q_l * \left(1 + \frac{R_p}{R_m}\right) \tag{2}$$

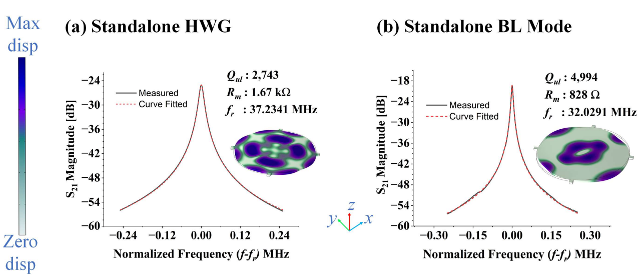

Figure 5: Measured S_{21} curve with the electrical parameters extracted through curve fitting, along with the displacement profile in inset for (a) the standalone HWG device, and (b) the standalone BL device.

Note that there is a slight difference in the resonance frequencies between the reference standalone and the tank mode devices, which is due to a slight difference in the central tank radius (200 µm compared to 230 µm). However, as it has been shown in previous work that within the 200-250 µm disk diameter range, the Q remains fairly constant for the HWG and BL modes [12], a comparison for Q enhancement remains valid.

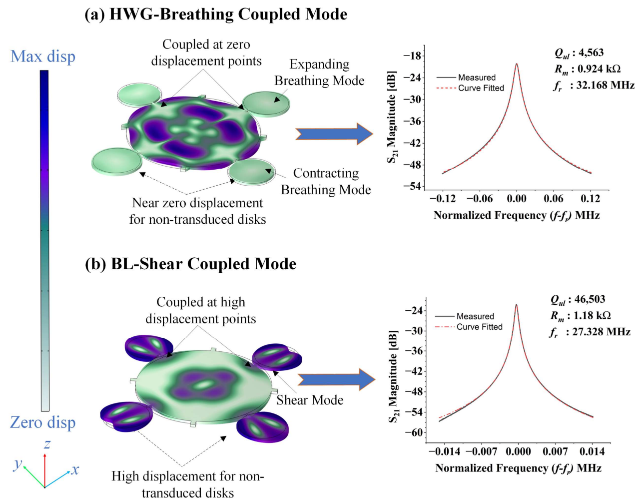

Figure 6: Measured S_{21} plots with the electrical parameters extracted through curve fitting, along with the displacement profiles for (a) the HWG tank with breathing modes coupled at the zero displacement points, resulting in weak movement for the SCS structures, and (b) the BL tank with the shear modes coupled at high displacement points for optimal energy sharing and higher Q_{ul}.

The standalone HWG and BL modes have Q_{ul} values of 2,794 and 4,994 respectively, with the higher strain confinement of the BL mode resulting in less energy dissipation, and consequently, less anchor movement resulting in a higher Q. The HWG-Breathing coupled mode has a performance enhancement of 1.6X compared to the standalone HWG mode with a Q_{ul} of 4,563, whereas the BL-Shear coupled mode has a near 10X improvement in its Q_{ul} compared to its standalone counterpart at 46,503. This difference in Q-enhancement was predicted in the design section, where the shear mode due to higher strain energy transference aids in the Q-boosting of the BL mode. However, another major reason can be observed from the displacement profiles in Fig. 6 as the HWG has been coupled at the low displacement points to the breathing modes, resulting in less movement. On the contrary, the BL mode has high displacement coupling with the shear modes, thus increasing energy sharing. This shows that the displacement profile along with the strain profile is critical for determining the correct coupling point in mechanically coupled devices for achieving Q-enhancement. On the motional resistance front, the HWG-Breathing coupled mode performs better than the BL-Shear coupled mode. The reason can be understood from the mode shapes of Fig. 2 (b), where the BL mode has a visibly weaker strain compared to the HWG, resulting in non-optimized mode extraction. This issue can be overcome by tuning the dimension of the central BL tank to improve the strength of the strain. Another possible reason could be that the electrode shapes depicted in Fig. 4 are more closely aligned with the HWG strain profile than that of the BL mode.

The influence of atmospheric pressure on the BL-Shear mode was obtained by periodically releasing the pressure within the vacuum chamber, as shown in Fig. 7. The mode has a high dependence on the ambient pressure, as a Q_{ul} drop of 2.5X is observed (19,338) as the pressure is increased from 90 mTorr to atmospheric pressure. This indicates a higher out-of-plane motion for the shear mode which results in slide-film damping in ambient air conditions. However, this value is still one of the highest in ambient air for TPoS resonators.

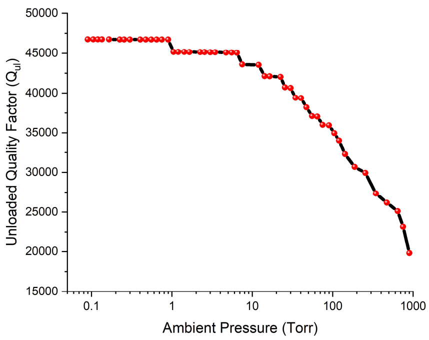

Figure 7: Variation in Q_{ul} of the BL-Shear coupled mode resonator as a function of ambient pressure.

CONCLUSIONS

In conclusion, this work successfully demonstrated a robust, lithographically defined methodology that significantly enhanced the quality factor through a BL-Shear coupled mode resonator, achieving nearly a tenfold Q improvement. As indicated by the comparative performance data presented in Table 2, the BL-Shear coupled mode exhibits one of the highest thickness-normalized unloaded quality factors in ambient air. This attribute renders it highly suitable for applications in low-noise oscillators or filters with minimal vacuum packaging requirements. The study has also highlighted two major design considerations for enhancing the quality factor through mechanical coupling: the choice of mode shape and the location of the couplers. Looking ahead, there is potential to further optimize the BL-Shear mode for a stronger strain profile, which could lead to a reduction in motional impedance and additional improvements in the quality factor.

Table 2. Comparison with high-performance related works on TPoS resonators

Ref	Device	f_o (MHz)	Device thickness (μm)	Q_{ul} (air)	Q_{ul} (vacuum)	R_m (Ω)
[5]	ScAlN on Si	19.7	40	-	172,105	350
[6]	AlN on Si	58.6	10	9,670	58,276	1250
[13]	AlN on Si	63.6	10	10,254	19,728	368
This work	AlN on Si	27.3	10	19,338	46,503	1180

ACKNOWLEDGEMENTS

The authors express their thanks to CMC Microsystems for the provision of the CAD tools and fabrication services that were essential in realizing this work. Appreciation is also extended to the Natural Sciences and Engineering Research Council (NSERC) and École de Technologie Supérieure (ETS) for their financial support.

REFERENCES

[1] R. Abdolvand, B. Bahreyni, J. Lee, and F. Nabki, “Micromachined Resonators: A Review,” *Micromachines*, vol. 7, no. 9, p. 160, Sep. 2016, doi: 10.3390/mi7090160.

[2] R. Abdolvand, H. Lavasani, G. Ho, and F. Ayazi, “Thin-film piezoelectric-on-silicon resonators for high-frequency reference oscillator applications,” *IEEE Trans. Ultrason., Ferroelect., Freq. Contr.*, vol. 55, no. 12, pp. 2596–2606, Dec. 2008, doi: 10.1109/TUFFC.2008.976.

[3] L.-W. Hung and C. T.-C. Nguyen, “Q-boosted AlN array-composite resonator with Q>10,000,” in *2010 International Electron Devices Meeting*, San Francisco, CA, USA: IEEE, Dec. 2010, p. 7.3.1-7.3.4. doi: 10.1109/IEDM.2010.5703315.

[4] S. Seth, S. Wang, T. Kenny, and B. Murmann, “A −131-dBc/Hz, 20-MHz MEMS oscillator with a 6.9-mW, 69-kΩ, gain-tunable CMOS TIA,” in *2012 Proceedings of the ESSCIRC (ESSCIRC)*, Sep. 2012, pp. 249–252. doi: 10.1109/ESSCIRC.2012.6341332.

[5] L. Huang, Z. Feng, Y. Xiao, F. Sun, and J. Xu, “High-Q and Low-Motional Impedance Piezoelectric mems Resonator through Mechanical Mode Coupling,” in *2023 IEEE 36th International Conference on Micro Electro Mechanical Systems (MEMS)*, Jan. 2023, pp. 1159–1162. doi: 10.1109/MEMS49605.2023.10052210.

[6] G. Pillai and S.-S. Li, “Quality factor boosting of bulk acoustic wave resonators based on a two dimensional array of high- Q resonant tanks,” *Applied Physics Letters*, vol. 116, no. 16, p. 163502, Apr. 2020, doi: 10.1063/5.0007418.

[7] A. Ali and J. E.-Y. Lee, “Piezoelectric transduction of a button-like mode disk resonator for enhanced quality factor in water,” in *2017 Joint Conference of the European Frequency and Time Forum and IEEE International Frequency Control Symposium (EFTF/IFCS)*, Jul. 2017, pp. 26–29. doi: 10.1109/FCS.2017.8088791.

[8] B. P. Harrington and R. Abdolvand, “In-plane acoustic reflectors for reducing effective anchor loss in lateral–extensional MEMS resonators,” *J. Micromech. Microeng.*, vol. 21, no. 8, p. 085021, Jul. 2011, doi: 10.1088/0960-1317/21/8/085021.

[9] A. Cowen, G. Hames, K. Glukh, and B. Hardy, “PiezoMUMPs design handbook,” *MEMSCAP Inc*, vol. 1, 2014.

[10] A. Ali and J. E.-Y. Lee, “Piezoelectric-on-Silicon Square Wine-Glass Mode Resonator for Enhanced Electrical Characterization in Water,” *IEEE Transactions on Electron Devices*, vol. 65, no. 5, pp. 1925–1931, May 2018, doi: 10.1109/TED.2018.2810700.

[11] G. Wu *et al.*, “Wafer-Level Vacuum-Packaged High-Performance AlN-on-SOI Piezoelectric Resonator for Sub-100-MHz Oscillator Applications,” *IEEE Transactions on Industrial Electronics*, vol. 65, no. 4, pp. 3576–3584, Apr. 2018, doi: 10.1109/TIE.2017.2748041.

[12] A. Ali and J. E.-Y. Lee, “Fully Differential Piezoelectric Button-Like Mode Disk Resonator for Liquid Phase Sensing,” *IEEE Trans. Ultrason., Ferroelect., Freq. Contr.*, vol. 66, no. 3, pp. 600–608, Mar. 2019, doi: 10.1109/TUFFC.2018.2872923.

[13] K. S. Sharma, H.-T. Jen, S.-S. Li, and G. Pillai, “Investigation of support transducer enabled higher-order radial bulk mode MEMS resonator and low phase noise oscillator,” *J. Micromech. Microeng.*, vol. 32, no. 8, p. 084004, Jul. 2022, doi: 10.1088/1361-6439/ac7bd1.

CONTACT

*F.Nabki, tel: (514) 396-8753; Email: frederic.nabki@etsmtl.ca